New Results

In silico stress fibre content affects peak strain in cytoplasm and nucleus but not in membrane for uniaxial substrate stretch

Tamer Abdalrahman[1,2], Neil H. Davies[3], Thomas Franz[1,4*]

[1]Division of Biomedical Engineering, Department of Human Biology, Faculty of Health Sciences, University of Cape Town, Observatory, South Africa

[2]Julius Wolff Institute for Biomechanics and Musculoskeletal Regeneration, Charité – Universitätsmedizin Berlin, Berlin, Germany

[3]Chris Barnard Division of Cardiothoracic Surgery, Faculty of Health Sciences, University of Cape Town, Observatory, South Africa

[4]Bioengineering Science Research Group, University of Southampton, Southampton, UK

*Corresponding author
Thomas Franz, PhD
Division of Biomedical Engineering
Department of Human Biology
Faculty of Health Sciences
University of Cape Town
Private Bag X3, Observatory 7935, South Africa
Tel.: +27 21 650 1795
Email: thomas.franz@uct.ac.za

Abstract

Introduction: Existing in silico models for single cells feature limited representations of cytoskeletal structures that present inhomogeneities in the cytoplasm and contribute substantially to the mechanical behaviour of the cell. Considering these microstructural inhomogeneities is expected to provide more realistic predictions of cellular and subcellular mechanics. Here, we propose a micromechanical hierarchical approach to capture the contribution of actin stress fibres to the mechanical behaviour of a single cell when exposed to substrate stretch.

Methods: For a cell-specific geometry of a fibroblast with membrane, cytoplasm and nucleus obtained from confocal micrographs, the Mori-Tanaka homogenization method was employed to account for cytoplasmic inhomogeneities and constitutive contribution of actin stress fibres. The homogenization was implemented in finite element models of the fibroblast attached to a planar substrate with 124 focal adhesions. With these models, the strains in cell membrane, cytoplasm and nucleus due to uniaxial substrate stretch of 1.1 were assessed for different stress fibre volume fractions in the cytoplasm of up to 20% and different elastic modulus of the substrate.

Results: A considerable decrease of the peak strain with increasing stress fibre content was observed in cytoplasm and nucleus but not the cell membrane, whereas peak strain increased in cytoplasm, nucleus and membrane for increasing elastic modulus of the substrate.

Conclusions: With the potential for extension, the developed method and models can contribute to more realistic in silico models of cellular mechanics.

Keywords: cell mechanics; stress fibres; cytoskeleton; micromechanical homogenization; Mori-Tanaka scheme; finite element modelling

Introduction

The knowledge of how the cell structure deforms under different loads is crucial for a better understanding of physiological and pathological events [1, 2]. The cell comprises different components (e.g. cytosol, fibrous protein networks, nucleus, cell membrane) that are dispersed heterogeneously, display nonlinear behaviour [3,4], and can be highly anisotropic. The cytoskeletal structural components determine the mechanical properties of the cell. These properties can be quantified through experimental characterisation and theoretical formulations [5, 6] and have been found to vary even for the same type of cell [7].

Various techniques have been developed to obtain the mechanical properties of cells, including micropipette aspiration [8], use of optical tweezers [9], magnetometric examination [10] and atomic force microscopy (AFM) based strategies [11,12].

The cytoskeleton, and the actin filaments in particular, are effective factors in the regulation of the morphology and mechanical properties of the cell; as such cytoskeletal changes associated with cellular remodelling may lead to substantial changes of the mechanical properties of a cell [14–17]. Park et al. [13] examined the localised cell stiffness and its correlation with the cytoskeleton. They reported that the local variation of cytoskeletal stiffness was related to regional prestress. This research comprehensively characterized the localized variations of intracellular mechanical properties that underlie localized cellular function.

Rotsch and Radmacher [18] found a significant reduction in the elastic modulus of fibroblasts when treated with actin disrupting chemicals. Similar findings were reported by other researchers [19, 20]. Variations in cellular stiffness has also been linked to diseases [21], e.g normal cells have an elastic modulus of about one order of magnitude higher than cancerous cells [22]. However, with some exceptions [23-26], in earlier research homogenization was applied to the whole cell and did not explicitly consider the effect of inhomogeneities [27]. This resulted in nonphysical relationships of the observed parameters to the mechanical properties of the cell.

In computational modelling of cell mechanics, an accurate description of the anisotropic, nonlinear behaviour of the cytoskeleton is desired to account for cytoplasmic inhomogeneity. One of the most common approaches for computational cell mechanics is the finite element method (FEM). FEM has been utilized to study different aspects of cell mechanics [28-30]. However, the application of FEM to single cell mechanics [31-33] is still limited because of the scarcity of information on material properties and shape of sub-cellular structures. More recently, image-based geometrical modelling and FEM have facilitated computational models that represent the three-dimensional (3D) cellular structures including cytoskeleton, cytoplasm, cell membrane, and nucleus [34-38]. However, including cytoskeletal stress fibres as discrete structural elements is one of the current challenges in computational models of cellular mechanics.

Multiscale constitutive models may be able to address this challenge by capturing the structural and mechanical properties of cellular components at sub-cellular scale and describing their mechanical contribution at the cellular scale.

Our current study focuses on developing a computational model to predict the mechanical behaviour of the cell via a multiscale approach. The micromechanical homogenization of actin stress fibres permits the combination of micro-structural details of these cytoskeletal components into the FEM modelling framework. This improves the capability of the framework to capture the contribution of the structure and mechanics at the microstructural sub-cellular level to the cellular mechanics at the macroscopic level.

Materials and methods

Geometrical modelling

The geometrical model of a human dermal fibroblast developed previously [30] was utilized in the current study. In brief, human dermal fibroblast cells were seeded onto fibronectin-coated sterile cover glasses. Cells were stained with Alexa Fluor 568 phalloidin (Invitrogen Molecular Probes, Eugene, Oregon, USA) and counterstained with Hoechst 33342 dye (Sigma Aldrich Chemie GmbH, Steinheim, Germany). Images were acquired with a Zeiss 510 LSM Meta confocal microscope at 40x magnification.

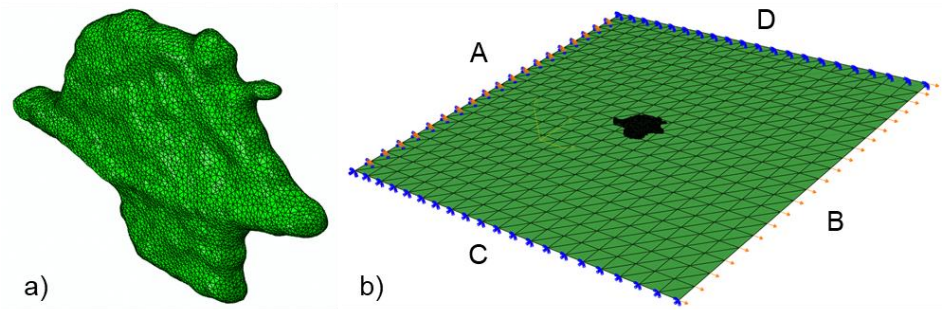

Figure 1*. a) 3D reconstructed and meshed geometry of the fibroblast. b) Cell attached to substrate. Boundary conditions of the substrate: Edge (A) fixed in all directions; uniaxial quasi-static displacement applied normally to opposite edge B; edges C and D free in direction of displacement and fixed in the normal direction.*

The geometries of the cytoplasm and the nucleus were reconstructed from the image data using threshold-based segmentation, meshed and converted to volumes (Simpleware ScanIP, Synopsys, Mountain View, CA, USA). The reconstructed cell geometry has average in-plane dimensions of 145 µm in the long axis and 92 µm in the short axis, and a thickness of 14 µm. The nucleus has an in-plane diameter of 19 µm and a maximum thickness of 3 µm. The cell geometry was complemented with 0.01 µm thick membrane enveloping the cytosol and the nucleus [39-41], see ***Figure 1***(a).

Finite element modelling

Mesh generation

The cell membrane, cytosol and nucleus were meshed and identified as separate element sets. No-slip conditions were enforced at interfaces between the cellular components in Simpleware. The cell geometry was imported into ABAQUS (version 12.2, Dassault Systèmes, RI, USA) and attached to a 1 × 1 mm flat substrate to simulate exposure of the cell to substrate stretch as in our previous study [30], see ***Figure 1***(b).

For the attachment of the cell to the substrate, 124 focal adhesions (FA) with a thickness of 1 µm [45-48] with average contact area of 1 μm^2 [48] were randomly distributed across the basal cell surface [30]. Cohesive elements were used to represent the FA [30, 42-44]. **Table 1** summarises element types and numbers for the various structures in the finite

element model.

Table 1. Types and number of elements for each component in the model

Component	Type of element	Number of elements
Nucleus	C3D4	1075
Cytosol	C3D4	47029
Plasma membrane	S3R	14832
Elastic substrate	S3	800
Focal adhesion	COH3D6	248

Boundary conditions and loading

The cell was placed in the centre of the substrate with sufficient distance to the substrate boundaries to neglect edges effects (***Figure 1***b). One edge (A) of the substrate was fixed in all directions and a uniaxial quasi-static displacement was applied normally to the opposite edge (B). The other two edges (C and D) remained free in the direction of the displacement and fixed in the normal directions. The applied displacement generated a uniform deformation field in the substrate with a tensile strain up to 10% (i.e. stretch λ = 1.1).

Material Properties

The finite element simulations were limited to strain field. The cell membrane was assumed to be isotropic linear-elastic. The nucleus and cytosol were assumed to be isotropic hyper-elastic compressible and described with a Neo-Hookean strain energy function [51-53]:

$$\psi = \frac{\mu}{2}(\bar{I_1} - 1) + \frac{k}{2}(J - 1) \tag{1}$$

where ψ is the strain energy per unit of reference volume, and μ is the shear modulus and k is the bulk modulus. $\bar{I_1}$ and J are the first and third invariant of the left Cauchy-Green deformation tensor, **P**, given by:

$$\mathbf{P} = \mathbf{F} \cdot \mathbf{F}^{\mathbf{T}} \tag{2}$$

where **F** is the deformation gradient tensor [54]. The substrate and focal adhesions were represented with an isotropic linear-elastic material model. All materials parameters are provided in **Table 2**.

Table 2. Mechanical properties of cell components, substrate, and focal adhesions.

Component	Constitutive law	Parameter
Nucleus	Hyperelastic	μ = 1.7 kPa, k = 16.4 kPa [55]
Cytosol	Hyperelastic	μ = 1 kPa, k = 9.7 kPa [51]
Stress fibre	Linear-elastic	E = 1.45 MPa, ν = 0.3 [32]
Membrane	Linear-elastic	E = 7 kPa, ν = 0.45 [56]
Focal adhesion	Linear-elastic	E = 10 kPa, ν = 0.3 [49, 50]
Elastic substrate	Linear-elastic	E_{sub} = 0.01, 0.14, 1, 10 MPa, ν = 0.45

Micromechanical homogenization of cytoplasm

The cytoplasm includes the structures enclosed by the cell membrane except the nucleus, and comprises the network of cytoskeletal filaments of actin fibres, microtubules, and intermediate filaments. However, the function and dynamic behaviour of the cytoskeleton differs according to organism and cell type. The stress fibres are higher-order cytoskeletal structures composed of bundles of actin filaments.

Here, we consider the microstructure of cytoplasm with randomly oriented stress fibres. The micromechanical homogenization allows to obtain the effective mechanical properties of cytoplasm by assuming the cytoplasm as composite of cytosol and stress fibres (see ***Figure 2***). Homogenization is achieved by replacing the heterogenous microstructure with an equivalent homogenized structure. The micromechanical homogenization of material properties is obtained considering a representative volume element (RVE). The RVE is a statistical representation of microstructure of material and must provide sufficient details of the micro-fields to enable an accurate sampling of the entire domain. The effective

mechanical properties of the cytoplasm are then obtained based on the volume fraction of the stress fibres.

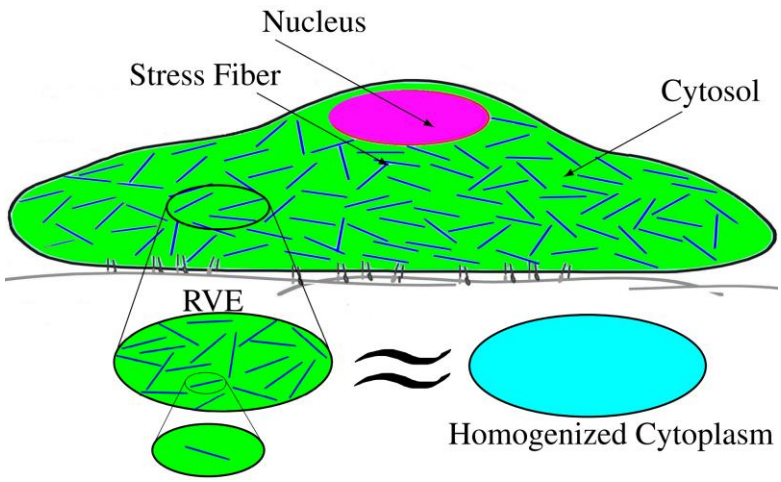

Figure 2*. Schematic cross-section of the cell illustrating the random distribution of several actin stress fibres and the corresponding homogenized microstructure.*

In microstructurally inhomogeneous materials, the volume average stress and strain, respectively, is obtained by integration of stress and strain, respectively, over the RVE volume with respect to microscopic coordinates inside the RVE:

$$< \sigma >= \frac{1}{\mathrm{V}} \int_V (\sigma)\, d\mathrm{V} \tag{3}$$

$$< \varepsilon >= \frac{1}{\mathrm{V}} \int_V (\varepsilon)\, d\mathrm{V} \tag{4}$$

Here, σ(x) and ε(x) are the microscopic stress and strain, respectively, which are related to the average stress and strain by:

$$\sigma(x) = \mathbf{A}(x) < \sigma > \tag{5}$$

$$\varepsilon(x) = \mathbf{B}(x) < \varepsilon > \tag{6}$$

where **A** and **B** are the stress and strain concentration tensors, respectively.

Based on complexity of the microstructure, the concentration tensors can be obtained by different approximations approaches. We consider a single ellipsoidal inclusion bonded to an infinite homogeneous elastic matrix that is subjected to a uniform strain and stress at infinity. For this problem, a suitable approximation approach is the mean field method, which is generally based on the Eshelby equivalent inclusion formulation [57]. The Mori-Tanaka (MT) homogenization model [58] is an effective field approximation based on Eshelby's elasticity solution, assuming that the strain concentration tensor, **B**, is equal to the strain concentration of the single inclusion problem. The Mori-Tanaka method is considered as an improvement over Eshelby method, and the relationship for the effective strain is given as

$$< \varepsilon >^{f} = \mathbf{B}^{\mathrm{Eshelby}} < \varepsilon >^{m}. \tag{7}$$

The concentration tensor ($\mathbf{B}^{\mathrm{Eshelby}}$) for Eshelby's equivalent inclusion is

$$\mathbf{B}^{\mathrm{Eshelby}} = \left[\mathbf{I} - \mathbf{S}\mathbf{M}^{\mathbf{m}}(\mathbf{E}^{f} - \mathbf{E}^{m})\right]^{-1}, \tag{8}$$

where **I** is the identity tensor, **S** is the Eshelby tensor [58], **E** is the elastic tensor, **M** is the compliance tensor, and υ is the volume fraction. The superscripts *f* and *m* refer to the fibre and matrix, respectively.

The Mori-Tanaka concentration tensor ($\mathbf{B}^{\mathrm{MT}}$) will be given as

$$\mathbf{B}^{\mathrm{MT}} = \mathbf{B}^{\mathrm{Eshelby}}\left[(1 - \upsilon_f)\mathbf{I} + \upsilon_f \mathbf{B}^{\mathbf{Eshelby}}\right]^{-1} \tag{9}$$

The relationship between the macroscopic stress $< \sigma >$ and strain $< \varepsilon >$ can be obtained by:

$$< \sigma > = \mathbf{E}^{\text{eff}} < \varepsilon > \tag{10}$$

where $\mathbf{E}^{\text{eff}}$ is the effective elastic tensor of the homogeneous material that can be obtained as a function of strain concentration tensor $\mathbf{B}^{\text{MT}}$. To computationally model cell mechanics, capturing the nonlinear deformation of the cytoplasm under large displacement is required. The Neo-Hookean material model has been used to describe the nonlinear stress strain behaviour of the homogenized cytoplasm.

The cytoplasm is considered as composition of randomly oriented stress fibres in matrix of cytosol. The cytosol matrix is assumed to be hyperelastic with an elastic modulus of 1 kPa, see **Table 2**. The mechanical properties obtained from stretch tests [33] were utilised for the stress fibres. The effective linear-elastic bulk modulus K^{eff} and shear modulus μ^{eff} of the cytosol matrix with randomly oriented and distributed stress fibres are given as:

$$K^{eff} = \frac{\upsilon_m K_m + \upsilon_f K_f \mathrm{B}_K^{\text{Eshelby}}}{\upsilon_m + \upsilon_f \mathrm{B}_K^{\text{Eshelby}}} \tag{11}$$

$$\mu^{eff} = \frac{\upsilon_m \mu_m + \upsilon_f \mu_f \mathrm{B}_\mu^{\text{Eshelby}}}{\upsilon_m + \upsilon_f \mathrm{B}_\mu^{\text{Eshelby}}} \tag{12}$$

where μ, K, and υ are the shear modulus, bulk modulus, and volume fraction, respectively, of the materials defined by subscripts f = fibre and m = matrix.

The stress is obtained by:

$$\sigma_{11} = \frac{4C_1}{3J^{5/3}}\left(\lambda^2 - \frac{J}{\lambda}\right) + 2D_1(J-1) \tag{13}$$

where $C_1 = \mu/2$, $D_1 = k/2$, and λ is the principal stretch.

Parametric numerical study

Changes in the actin cytoskeletal structure have been reported to affect cell fate [19]. The mechanical properties of different cellular components, such as the elastic moduli of nucleus, cytoplasm, actin cortex and actin stress fibres, contribute to the effective

mechanical stiffness of the cell [40].

Parametric simulations were conducted to study the effect of stress fibre content and substrate elasticity on the deformation of the cell. The volumetric fraction of filamentous F-actin in the cytoskeleton has been reported to be of the order of 1% [59]. Since we expect the stress fibre volume fraction in actin-rich regions intracellular regions (such as the cortex or actin bundles) to be higher than normal, we considered networks with stress fibre volume fractions of $\upsilon_f = 0$, 1, 10, and 20%. Furthermore, we considered an elastic modulus of the substrate of $E_S = 0.01$, 0.14, 1 and 10 MPa. The reference mechanical properties of the cell are summarised in **Table 2**. The computed strain in plasma membrane, homogenised cytoplasm and nucleus of the cell exposed to uniaxial stretch as described above were assessed.

Results

Homogenization of cytoplasm

Figure 3 illustrates the relationship between the effective mechanical properties of the homogenised cytoplasm and the stress fibre volume fraction. The shear modulus μ^{eff}, bulk modulus K^{eff} and effective elastic modulus E^{eff} increase with increasing stress fibre volume fraction υ_f whereas the Poisson's ratio decreases for increasing stress fibre volume fraction.

The stress-stretch relationship for the macroscopic behaviour of the homogenized cytoplasm is illustrated in ***Figure 4***(a) for different stress fibre volume fractions. An increase in stress fibre volume fraction resulted in an increase in stress for a given stretch. For small stretch values of $\lambda \leq 1.1$, the stress-stretch relationship can be approximated as linear (see ***Figure 4***b).

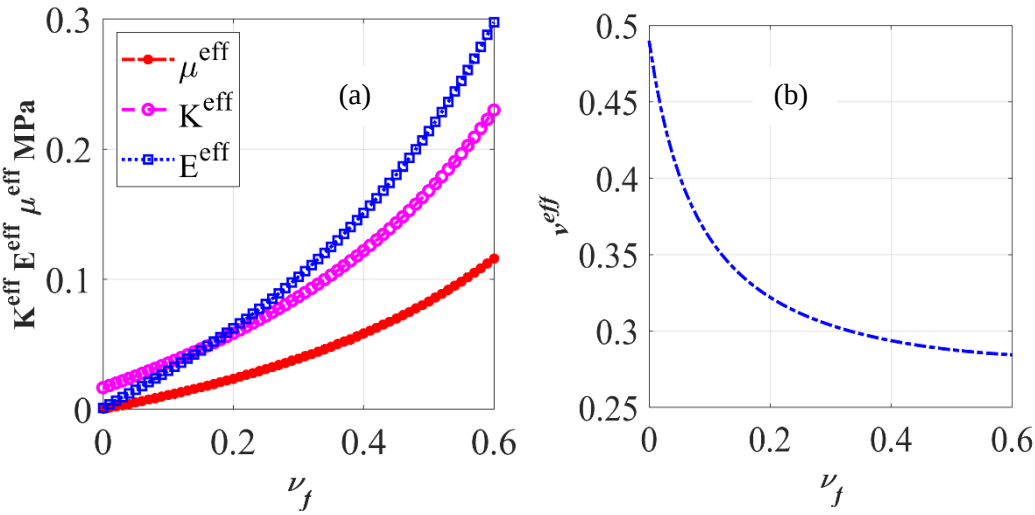

Figure 3. *The effect of stress fibre volume fraction v_f on (a) the effective elastic modulus* $\boldsymbol{E}^{eff}$, *shear modulus* $\boldsymbol{\mu}^{eff}$ *and bulk modulus* $\boldsymbol{K}^{eff}$, *and (b) the effective Poisson's ratio of the homogenised cytoplasm.*

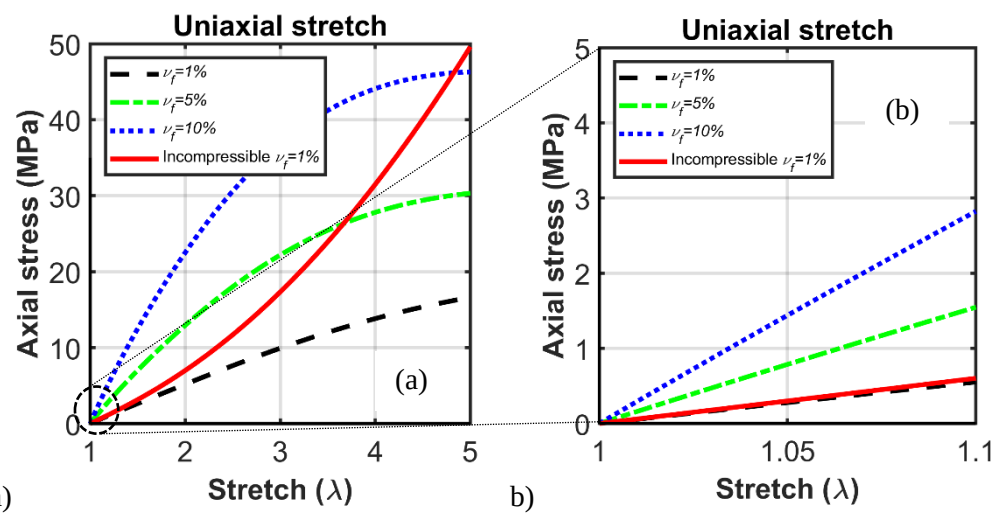

Figure 4. *The true maximum principal stress as a function of uniaxial stretch for the homogenised cytoplasm predicted by hyperelastic* constitutive laws of *Neo-Hookean material model for large stretch λ = 1.0 to 5.5 (a) and for small stretch λ = 1.0 to 1.1 (b).*

Effect of stress fibre volume fraction and substrate modulus on cell deformation

The predicted distribution of the maximum principal strain in the mid plane of the cytoplasm and nucleus is presented in ***Figure 5***. The results are shown in the mid plane of the cytoplasm to disregard potential numerical localization effects of the contact between the cell and the substrate. The intracellular strain distribution, i.e. spatial pattern, was found to be insensitive to variation of the stress fibre volume fraction, whereas different strain magnitudes were apparent for the different cases. It was also noted that the peak strain in the cytosol and nucleus decreased considerably with including stress fibres.

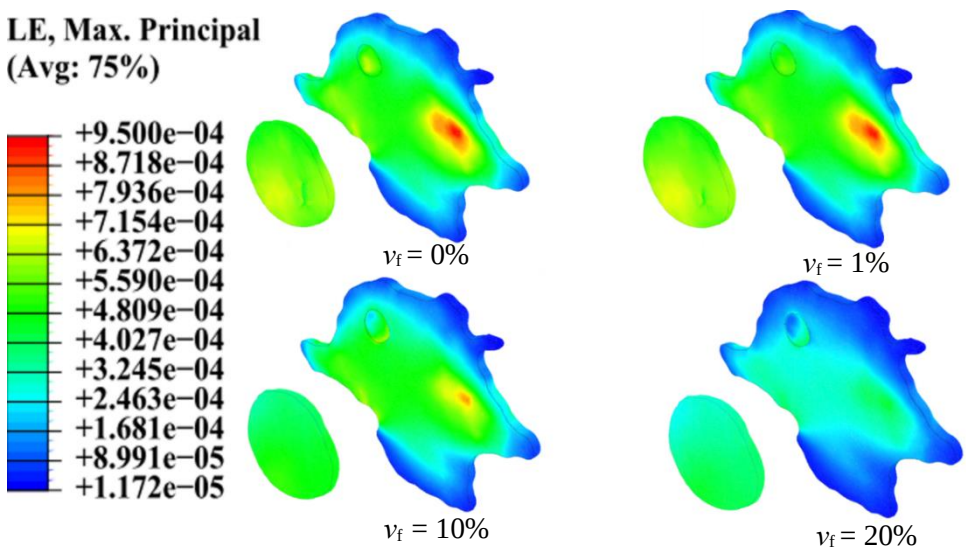

Figure 5*. Distribution of maximum principal strain in the mid-section of cytoplasm and nucleus for E_{sub} = 0.01 MPa at different stress fibre volume fractions υ_f = 0, 1, 10 and 20%.*

Figure 6 illustrates the peak maximum principal strain in the mid-section of the cell (as illustrated in ***Figure 5***) versus stress fibre volume fraction and substrate elastic modulus for cytoplasm, nucleus and membrane. With increasing stress fibre volume fraction υ_f, the strain decreased in the cytoplasm and in the nucleus whereas it did not change considerably in the cell membrane. A consistent response of cytoplasm and nucleus was also observed in the strain sensitivity to the change of υ_f. The change in stress fibre volume fraction had a negligible effect on the peak strain in the membrane, ***Figure 6***c. The peak strain in all

three cell components increased with increasing elastic modulus of the substrate, E_{sub} (***Figure 6***). The changes in peak strains in the cell were larger for changes in the lower range of E_{sub}, where it is of the same order of magnitude as the elastic modulus of the cell components, compared to the upper region of E_{sub} where the elastic modulus of the substrate is much higher than that of the cell components.

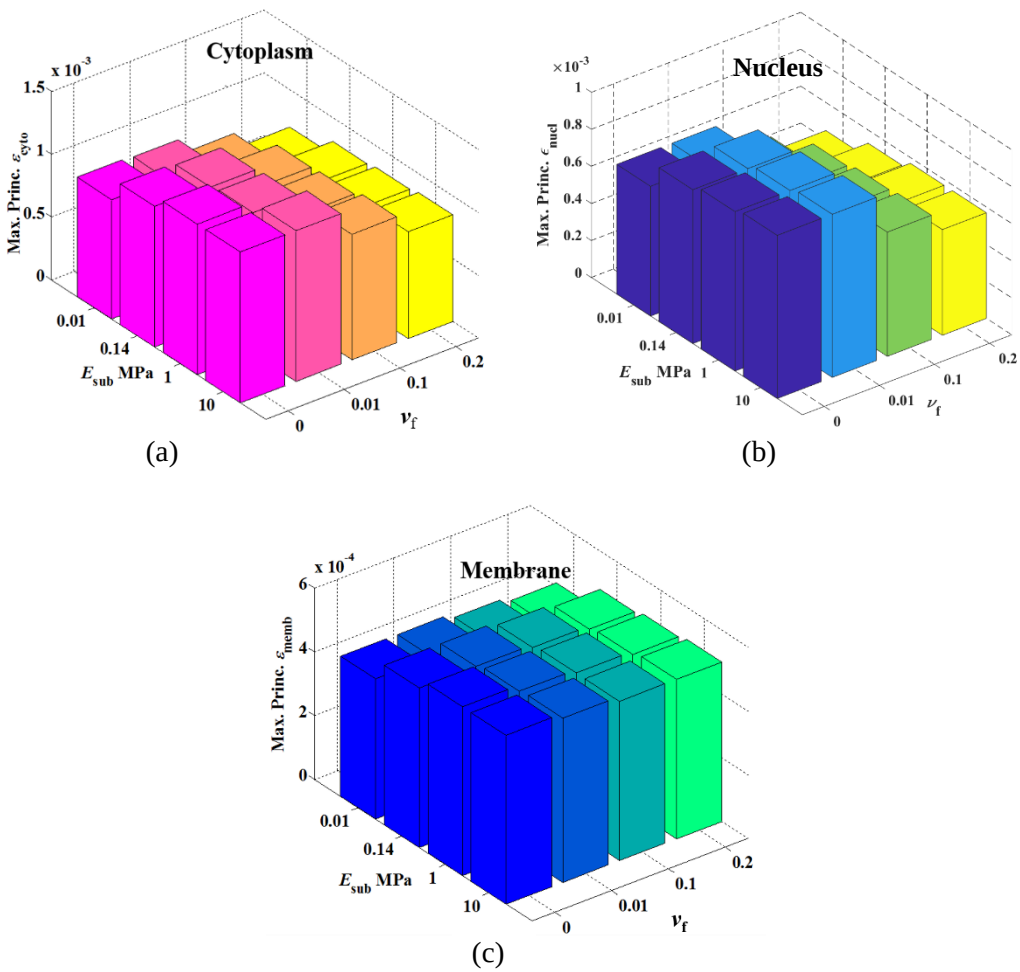

Figure 6*. Peak maximum principal strain in the mid-section of cytoplasm (a), nucleus (b) and membrane (c) at a substrate stretch of $\lambda = 1.1$ for different ν_f and E_{sub}. (The values of the peak maximum principal strains in cytoplasm, nucleus and cell membrane are provided in the online supplement,* ***Table S1****).*

Figure 7 and ***Figure 8*** provide graphs of overall peak maximum principal logarithmic strain in the cytoplasm $\varepsilon_{1,Peak,Cyt}$ and the nucleus $\varepsilon_{1,Peak,Nuc}$ versus the peak maximum

principal strain in the substrate $\varepsilon_{1,Peak,Sub}$ for different stress fibre volume fractions and substrate elastic moduli. (Here, 'overall strain' refers to the strain in the entire cytoplasm and nucleus in contrast to the strain in the mid-section presented in **Figure 5** and **Figure 6**.) The overall peak strain in the cytoplasm increased linearly with increasing strain in the substrate. The overall peak strain in the nucleus also increased linearly with increasing substrate strain, however, without a gradient change of the curve.

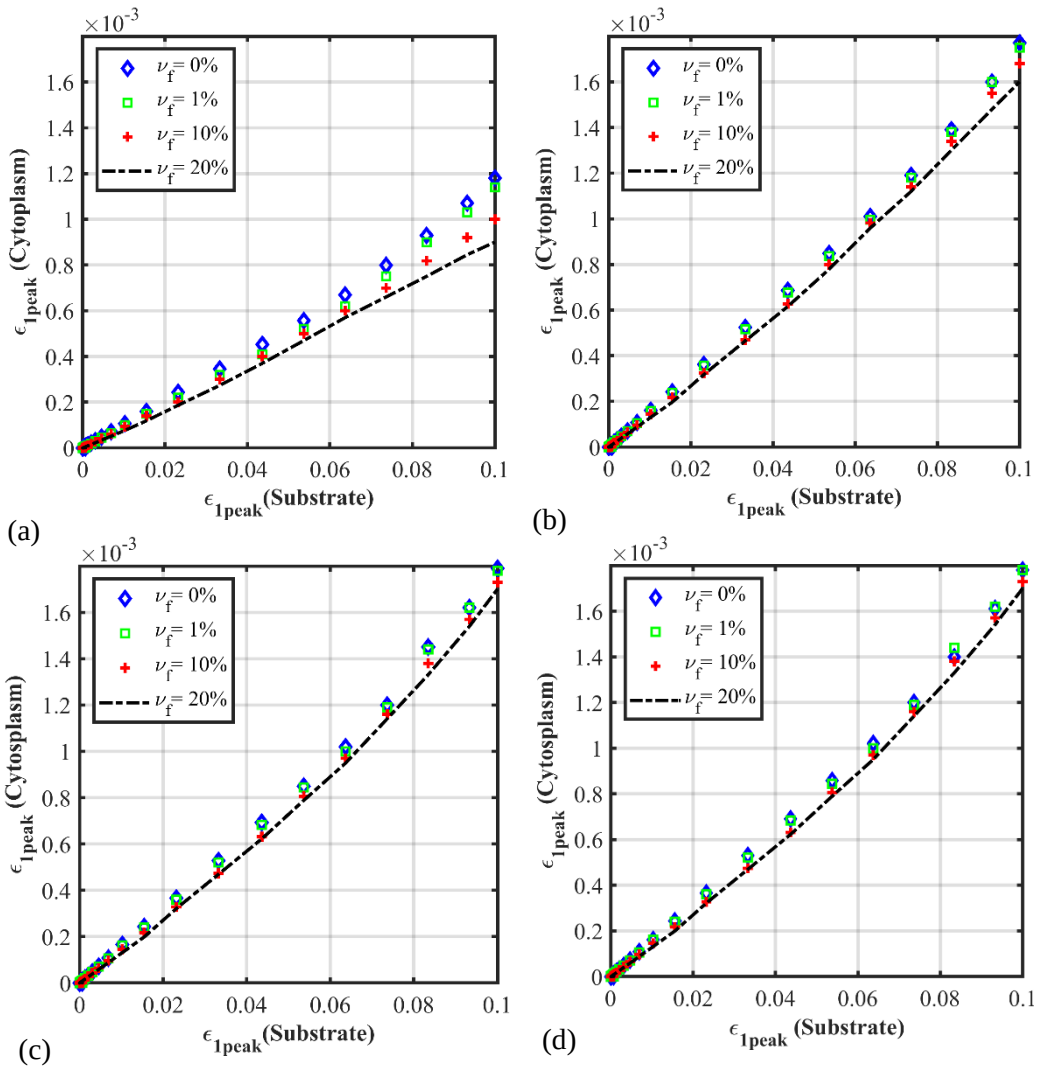

***Figure 7**. Overall peak maximum principal strain in cytoplasm versus same strain in substrate for different stress fibre volume fractions of 0, 1, 10 and 20% for the substrate elastic modulus E_{sub} of 0.01 MPa (a), 0.14 MPa (b), 1 MPa (c) and 10 MPa (d).*

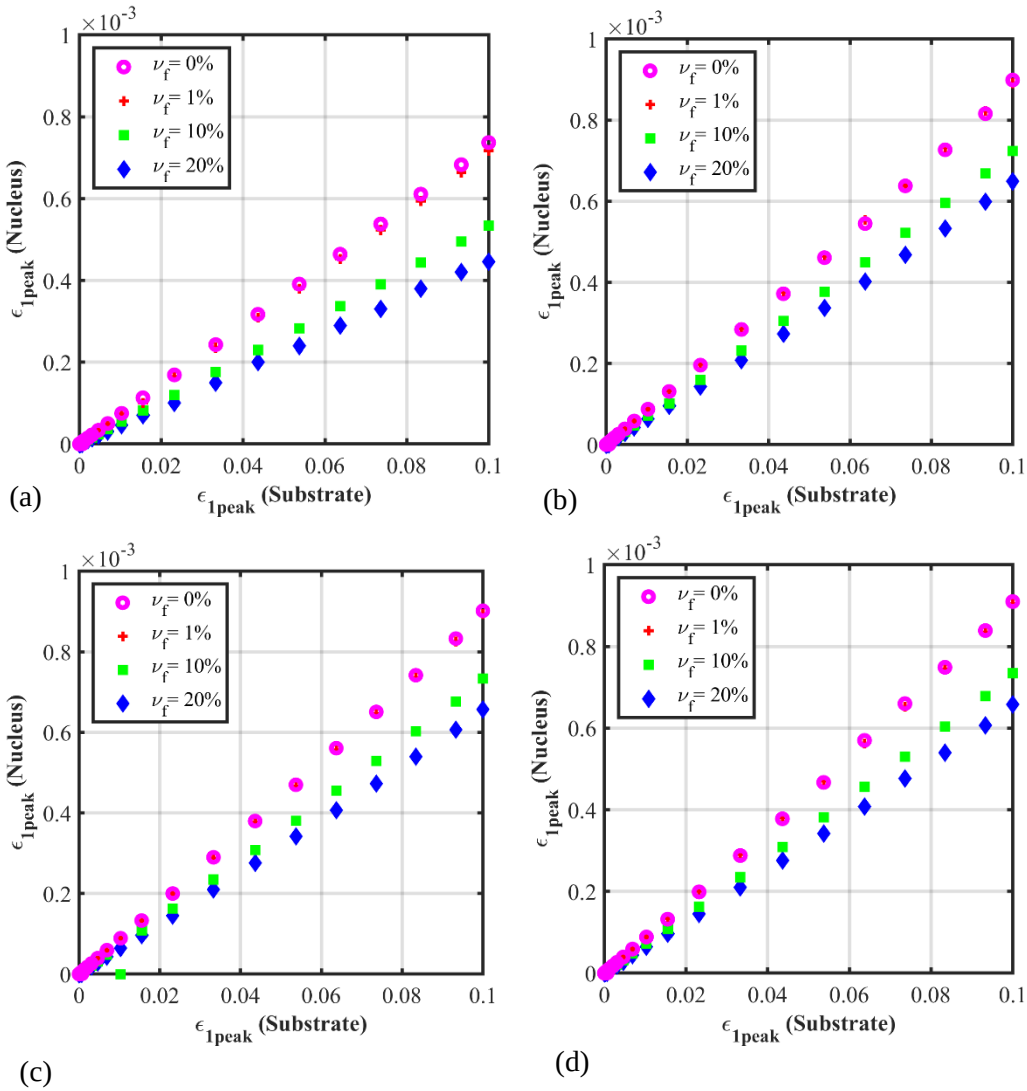

***Figure 8**. Overall peak maximum principal strain in nucleus versus the same strain in the substrate for different stress fibre volume fractions of 0, 1, 10 and 20% and substrate elastic modulus E_{sub} of 0.01 MPa (a), 0.14 MPa (b), 1 MPa (c) and 10 MPa (d).*

The relationship between the overall peak strain in the cytosol and nucleus, respectively, and the overall peak strain in the substrate can be approximated with linear functions for the cytosol,

$$\epsilon_{1,Peak,Cyt} = \alpha_{Cyt} \cdot \epsilon_{1,Peak,Sub} + \beta_{Cyt} \tag{14}$$

and the nucleus

$$\epsilon_{1,Peak,Nuc} = \alpha_{Nuc} \cdot \epsilon_{1,Peak,Sub} + \beta_{Nuc} \,. \tag{15}$$

The values for parameters α and β for nucleus and cytoplasm for different values of the substrate elastic modulus and the stress fibre volume fraction are provided in **Table 3**.

Table 3. Parameter values for estimation of overall peak strain in cytoplasm and nucleus (see Eqs. 14 and 15).

E_{sub} (MPa)		Cytoplasm υ_f 0%	1%	10%	20%		Nucleus υ_f 0%	1%	10%	20%
0.01	α_{Cyt}	0.0112	0.0107	0.0096	0.009	α_{Nuc}	0.0073	0.0071	0.0053	0.0045
	β_{Cyt}	$-5e^{-6}$	$-6e^{-6}$	$-4e^{-6}$	$-4e^{-6}$	β_{Nuc}	$-5e^{-7}$	$-8e^{-7}$	$-5e^{-7}$	$-2e^{-7}$
0.14	α_{Cyt}	0.0168	0.0167	0.016	0.0156	α_{Nuc}	0.0088	0.0087	0.0072	0.0064
	β_{Cyt}	$-8e^{-6}$	$-8e^{-6}$	$-1e^{-5}$	$-1e^{-5}$	β_{Nuc}	$-1e^{-7}$	$-1e^{-7}$	$-1e^{-7}$	$-1e^{-7}$
1	α_{Cyt}	0.017	0.17	0.0164	0.0161	α_{Nuc}	0.0089	0.0088	0.0073	0.0065
	β_{Cyt}	$-8e^{-6}$	$-9e^{-6}$	$-1e^{-5}$	$-1e^{-5}$	β_{Nuc}	$-2e^{-7}$	$-1e^{-7}$	$-4e^{-7}$	$-1e^{-7}$
10	α_{Cyt}	0.169	0.169	0.0163	0.0156	α_{Nuc}	0.009	0.0089	0.0073	0.0065
	β_{Cyt}	$-7e^{-6}$	$-8e^{-6}$	$-1e^{-5}$	$-1e^{-5}$	β_{Nuc}	$-3e^{-7}$	$-2e^{-7}$	$-1e^{-7}$	$-1e^{-7}$

Discussion

Previous research of eukaryotic cells has shown that the cytoskeletal structures determine to a great extent the distinct mechanical properties of the cytoplasm. In some of computational modelling studies of single cell mechanics, the assumption of homogenous mechanical properties for the entire cell has been a strong simplification particularly for cells with focal adhesions where stress fibre presents critical inhomogeneity. Hybrid computational cell models [37, 38, 39] with a restricted number of tensegrity elements to represent the mechanical contribution of stress fibres have remained limited in their capabilities to capture real cellular behaviour. One of the main shortcomings of continuum

based models is the lack of representation of the functional contribution of cytoskeletal fibres [60].

In our current study, we developed a finite element method and models for single cell mechanics with the micromechanical homogenization of actin stress fibres as primary cytoskeletal elements in the cytoplasm. The method and models were used to investigate the influence of stress fibre content on the deformation of cytoplasm, nucleus and cell membrane of a fibroblast when subjected to uniaxial strain of up to 10% on substrates of different stiffness.

This study demonstrates the importance of the representation of cytoskeletal components in computational models for single cell mechanics since the predicted intracellular strains varied substantial for different stress fibre contents.

The data for stress fibre volume fractions of 0% and 20% indicated that an increase in stress fibre volume fraction led to a decrease in the peak strain in cytoplasm and nucleus but did not affect the strain in cell membrane to the same degree (**Figure 6**). As shown in **Figure 5**, the spatial distribution of strain is similar for the four cases of our study because the focal adhesions have identical distribution for all cases. We have investigated the effect of focal adhesions on intracellular strain distribution in previous studies [30, 61, 62].

It was also observed that the mid-section peak strain in cytoplasm and nucleus decreased more for the change of stress fibre volume fraction from 0% to 10% than for the change from 10% to 20%. This effect, which was more pronounced in the nucleus than in the cytoplasm, suggesting that an increase in stress fibre content may lead to a decrease of mechanosensitivity. The negligible change of the strain in the cell membrane indicates that the membrane is less sensitive to a change in stress fibre content than the cytosol and nucleus.

Our findings also indicate that omission of stress fibres content may overestimate intracellular strain. Due to the challenges in discretely reconstructing the stress fibres for cellular modelling, numerous researches utilized beam elements to represent stress fibres [8, 9, 35, 37, 63]. However, this is not sufficient to represent the global effect of stress fibres for high volume fractions [64] and random orientations [65]. Our method with

micromechanical homogenization offers a new approach to address this limitation in single cell computational mechanics.

A substantial variation of the effective Poisson's ratio of the micromechanically homogenised cytoplasm was predicted for the change in stress fibre content (**Figure 3**). This is of interest in the context of the wide range of values reported in literature for Poisson's ratio, from nearly incompressible hyperelastic with 0.49 [66] to 0.3 [67, 68].

Numerical relationships were identified between overall peak strain in the cytosol and the nucleus, respectively, and the substrate strain (**Figure 7** and **Figure 8**) for varying stress fibre volume fraction and elastic modulus of the substrate. Once validated, such relationships can provide simple tools to estimate the maximum deformation in cellular components for a given stiffness of the extracellular environment, and consequently a design tool for cellular microenvironments to guide cellular deformation in therapeutic applications.

The hyperelastic response of the cytoplasm was captured by a Neo-Hookean strain energy density function based on isotropic elastic shear modulus and bulk modulus that were derived with by micromechanical homogenization. Based on the spread morphology of the fibroblast with a multitude of stress fibre orientations observed microscopically, the homogenized cytoplasm was treated as mechanically isotropic with randomly aligned stress fibres.

Shortcomings of the current study include the lack of quantitative information on the distribution of stress fibres within the cell and the omission of microtubules and intermediate filaments in the micromechanical homogenization of cytoskeletal structures. This was based on the technical challenge to identify these structures in the microscopic images. A further limitation is the lack of validation of the numerical results. However, at present, there is a scarcity of experimental data of cellular and subcellular physical parameters (e.g. mechanical properties of FA, structure and mechanical properties of cytoskeletal components) and on localized intracellular deformation such as provided by the FE models in this study (**Figure 5**).

Conclusion

This study demonstrated that the representation of stress fibres should be considered in computational models for cell mechanics since predicted cytoplasm elastic modulus values changed substantially with stress fibres content. The results also show that the stress fibres content influences the deformation of cytoplasm and nucleus but not of the membrane, at least for uniaxial substrate stretch. These developed methods and models offer potential for refinement and extension, for example to capture the regional variability of cytoskeletal content and mechanical anisotropy of the cytoplasm. This study can as such contribute to the development of more realistic and accurate computational models of cell mechanics based on continuum approaches that will provide a better understanding of mechanotransduction in living cells.

Acknowledgements

The research reported in this publication was supported by the National Research Foundation of South Africa (UID 92531 and 93542), and the South African Medical Research Council under a Self-Initiated Research Grant (SIR 328148). Views and opinions expressed are not those of the NRF or MRC but of the authors.

Conflict of Interest

The authors declare that they have no conflicts of interest.

Data

Abaqus input files of the finite element models used in this study are available on are available on ZivaHUB (http://doi.org/10.25375/uct.9782798).

References

[1] Huang H, Kamm RD, Lee RT (2004) Cell mechanics and mechanotransduction: pathways, probes, and physiology. American Journal of Physiology-Cell Physiology 287(1):C1-11.

[2] Brown TD (2000) Techniques for mechanical stimulation of cells in vitro: a review. Journal of biomechanics 33(1):3-14. .

[3] Wang N, Naruse K, Stamenović D, Fredberg JJ, Mijailovich SM, Tolić-Nørrelykke IM, Polte T, Mannix R, Ingber DE (2001) Mechanical behaviour in living cells consistent with the tensegrity model. Proceedings of the National Academy of Sciences 98(14):7765-70.

[4] Moeendarbary E, Harris AR (2014) Cell mechanics: principles, practices, and prospects. Wiley Interdisciplinary Reviews: Systems Biology and Medicine 6(5):371-88.

[5] Karcher H, Lammerding J, Huang H, Lee RT, Kamm RD, Kaazempur-Mofrad MR (2003) A three-dimensional viscoelastic model for cell deformation with experimental verification. Biophysical journal 85(5):3336-49.

[6] Ohayon J, Tracqui P (2005) Computation of adherent cell elasticity for critical cell-bead geometry in magnetic twisting experiments. Annals of biomedical engineering. 33(2):131-41.

[7] Evans ND, Gentleman E (2014) The role of material structure and mechanical properties in cell–matrix interactions. Journal of Materials Chemistry B 2(17):2345-56.

[8] Barreto S, Clausen CH, Perrault CM, Fletcher DA, Lacroix D (2013) A multi-structural single cell model of force-induced interactions of cytoskeletal components. Biomaterials 34(26):6119-26. .

[9] Barreto S, Perrault CM, Lacroix D (2014) Structural finite element analysis to explain cell mechanics variability. Journal of the Mechanical Behavior of biomedical materials 38:219-31.

[10] Ishiko A, Shimizu H, Kikuchi A, Ebihara T, Hashimoto T, Nishikawa T (1993) Human autoantibodies against the 230-kD bullous pemphigoid antigen (BPAG1) bind only to the intracellular domain of the hemidesmosome, whereas those against the 180-kD bullous pemphigoid antigen (BPAG2) bind along the plasma membrane of the hemidesmosome in normal human and swine skin. The Journal of Clinical Investigation 91(4):1608-15.

[11] Chen A, Moy VT (2000) Cross-linking of cell surface receptors enhances cooperativity of molecular adhesion. Biophysical Journal 78(6):2814-20.

[12] Thomas G, Burnham NA, Camesano TA, Wen Q (2013) Measuring the mechanical properties of living cells using atomic force microscopy. Journal of Visualized Experiments 27(76):e50497.

[13] Park CY, Tambe D, Alencar AM, Trepat X, Zhou EH, Millet E, Butler JP, Fredberg JJ (2010) Mapping the cytoskeletal prestress. American Journal of Physiology-Cell Physiology 298(5):C1245-52.

[14] Sosa MS, Bragado P, Aguirre-Ghiso JA (2014) Mechanisms of disseminated cancer cell dormancy: an awakening field. Nature Reviews Cancer 14(9):611.

[15] Mavrakis M, Azou-Gros Y, Tsai FC, Alvarado J, Bertin A, Iv F, Kress A, Brasselet S, Koenderink GH, Lecuit T (2014) Septins promote F-actin ring formation by crosslinking actin filaments into curved bundles. Nature cell biology 16(4):322.

[16] Lancaster OM, Baum B (2014) Shaping up to divide: coordinating actin and microtubule cytoskeletal remodelling during mitosis. InSeminars in cell & developmental biology 34:109-115.

[17] Stewart MP, Toyoda Y, Hyman AA, Müller DJ (2012) Tracking mechanics and volume of globular cells with atomic force microscopy using a constant-height clamp. Nature Protocols 7(1):143–154.

[18] Rotsch C, Radmacher M (2000) Drug-induced changes of cytoskeletal structure and mechanics in fibroblasts: an atomic force microscopy study. Biophysical Journal 78(1):520-35.

[19] Fletcher DA, Mullins RD. Cell mechanics and the cytoskeleton. Nature. 2010 Jan 27;463(7280):485.

[20] Wu, H. W., Kuhn, T., and Moy, V. T., 1998, "Mechanical Properties of L929 Cells Measured by Atomic Force Microscopy: Effects of Anticytoskeletal Drugs and Membrane Crosslinking," Scanning, 20 , pp. 389–397.

[21] Janmey PA, Miller RT. Mechanisms of mechanical signaling in development and disease. J Cell Sci. 2011 Jan 1;124(1):9-18.

[22] Lekka, M., Laidler, P., Gil, D., Lekki, J., Stachura, Z., and Hrynkiewicz, A. Z., 1999, "Elasticity of Normal and Cancerous Human Bladder Cells Studied by Scanning Force Microscopy," Eur. Biophys. J., 28, pp. 312–316.

[23] Na, S., Sun, Z., Meininger, G. A., and Humphrey, J. D., 2004, "On Atomic Force Microscopy and the Constitutive Behaviour of Cells," Biomech. Model Mechanobiol., 3, pp. 75–84.

[24] Karcher, H., Lammerding, J., Huang, H., Lee, R. T., Kamm, R. D., and Kaazempur-Mofrad, M. R., 2003, "A Three-Dimensional Viscoelastic Model for Cell Deformation With Experimental Verification," Biophys. J., 85, pp. 3336—3349.

[25] Ohayon, J., and Tracqui, P., 2005, "Computation of Adherent Cell Elasticity for Critical Cell-Bead Geometry in Magnetic Twisting Experiments," Ann. Biomed. Eng., 33, pp. 131–141.

[26] Humphrey, J. D., 2002, "On Mechanical Modeling of Dynamic Changes in Structure and Properties in Adherent Cells," Math. Mech. Solids, 7, pp. 521– 539.

[27] Lim CT, Zhou EH, Quek ST. Mechanical models for living cells—a review. Journal of biomechanics. 2006 Jan 1;39(2):195-216.

[28] Lavagnino M, Arnoczky SP, Kepich E, Caballero O, Haut RC (2008) A finite element model predicts the mechanotransduction response of tendon cells to cyclic tensile loading. Biomechanics and modeling in mechanobiology 7, 405-416.

[29] Miller P, Hu L, Wang J (2010) Finite element simulation of cell–substrate decohesion by laser-induced stress waves. Journal of the mechanical behaviour of biomedical materials 3:268–277.

[30] Abdalrahman T, Dubuis L, Green J, Davies N, Franz T. Cellular mechanosensitivity to substrate stiffness decreases with increasing dissimilarity to cell stiffness. Biomechanics and modeling in mechanobiology. 2017 Dec 1;16(6):2063-75.

[31] Simon BR, Kaufmann MV, McAfee MA, Baldwin AL (1993) Finite element models for arterial wall mechanics. Journal of Biomechanical Engineering 115:489–496

[32] Milner JS, Grol MW, Beaucage KL, Dixon SJ, Holdsworth DW (2012) Finite-element modeling of viscoelastic cells during high-frequency cyclic strain. Journal of Functional Biomaterials 3:209–224

[33] Mullen CA, Vaughan TJ, Voisin MC, Brennan MA, Layrolle P, McNamara LM (2014) Cell morphology and focal adhesion location alters internal cell stress. Journal of The Royal Society Interface 11:20140, 885.

[34] Verbruggen SW, Vaughan TJ, McNamara LM (2012) Strain amplification in bone mechanobiology: a computational investigation of the in vivo mechanics of osteocytes. Journal of the Royal Society Interface 9:2735–2744

[35] Barreto S, Clausen CH, Perrault CM, Fletcher DA, Lacroix D (2013) A multi-structural single cell model of force-induced interactions of cytoskeletal components. Biomaterials 34:6119–6126.

[36] Barreto S, Perrault CM, Lacroix D (2014) Structural finite element analysis to explain cell mechanics variability. Journal of the Mechanical Behaviour of Biomedical Materials 38:219–23.

[37] Slomka N, Gefen A (2010) Confocal microscopy-based three-dimensional cell-specific modeling for large deformation analyses in cellular mechanics. Journal of Biomechanics 43:1806–1816

[38] Slomka N, Gefen A (2012) Relationship between strain levels and permeability of the plasma membrane in statically stretched myoblasts. Annals of Biomedical Engineering 40:606–618

[39] Yao Y, Lacroix D, Mak AFT (2016) Effects of oxidative stress-induced changes in the actin cytoskeletal structure on myoblast damage under compressive stress: confocal-based cell-specific finite element analysis. Biomechanics and Modeling in Mechanobiology 15:1495-1508

[40] Chen A, Moy VT (2000) Cross-linking of cell surface receptors enhances cooperativity of molecular adhesion. Biophysical Journal 78:2814–2820

[41] Hine R (2009) The Facts on File Dictionary of Biology. Infobase Publishing

[42] Ishiko A, Shimizu H, Kikuchi A, Ebihara T, Hashimoto T, Nishikawa T (1993) Human autoantibodies against the 230-kd bullous pemphigoid antigen (BPAG1) bind only to the intracellular domain of the hemidesmosome, whereas those against the 180-kD bullous pemphigoid antigen (BPAG2) bind along the plasma membrane of the hemidesmosome in normal human and swine skin. Journal of Clinical Investigation 91:1608–1615

[43] Park K, Paulino GH (2012) Computational implementation of the PPR potential-based cohesive model in ABAQUS: educational perspective. Engineering Fracture Mechanics. 93:239-62.

[44] Dávila CG, Camanho PP, Turon A (2008) Effective simulation of delamination in aeronautical structures using shells and cohesive elements. Journal of Aircraft. 45:663-72

[45] Fortino S, Zagari G, Mendicino AL, Dill-Langer G (2012) A simple approach for FEM simulation of Mode I cohesive crack growth in glued laminated timber under short-term loading. Journal of Structural Mechanics 45:1-20.

[46] Bartalena G, Loosli Y, Zambelli T, Snedeker JG (2012) Biomaterial surface modifications can dominate cell–substrate mechanics: the impact of PDMS plasma treatment on a quantitative assay of cell stiffness. Soft Matter 8:673-81.

[47] Balaban NQ, Schwarz US, Riveline D, Goichberg P, Tzur G, Sabanay I, Mahalu D, Safran S, Bershadsky A, Addadi L, Geiger B (2001) Force and focal adhesion assembly: a close relationship studied using elastic micropatterned substrates. Nature Cell Biology 3(5):466..

[48] Goffin JM, Pittet P, Csucs G, Lussi JW, Meister JJ, Hinz B (2006) Focal adhesion size controls tension-dependent recruitment of α-smooth muscle actin to stress fibers. Journal of Cell Biology 172:259-68.

[49] Lelidis I, Joanny JF (2013) Interaction of focal adhesions mediated by the substrate elasticity. Soft Matter 9(46):11120-8.

[50] Nicolas A, Safran SA (2006) Limitation of cell adhesion by the elasticity of the extracellular matrix. Biophysical Journal 91(1):61-73.

[51] Engler AJ, Griffin MA, Sen S, Bönnemann CG, Sweeney HL, Discher DE (2004) Myotubes differentiate optimally on substrates with tissue-like stiffness: pathological implications for soft or stiff microenvironments. Journal of Cell Biology 166(6):877-87.

[52] Breuls RG, Sengers BG, Oomens CW, Bouten CV, Baaijens F (2002)Predicting local cell deformations in engineered tissue constructs: a multilevel finite element approach. Journal of Biomechanical Engineering 124(2):198-207.

[53] Baaijens FP, Trickey WR, Laursen TA, Guilak F (2005)Large deformation finite element analysis of micropipette aspiration to determine the mechanical properties of the chondrocyte. Annals of Biomedical Engineering 33(4):494-501.

[54] Peeters EA, Oomens CW, Bouten CV, Bader DL, Baaijens FP (2005) Mechanical and failure properties of single attached cells under compression. Journal of Biomechanics 38(8):1685-93.

[55] Jean RP, Chen CS, Spector AA (2005) Finite-element analysis of the adhesion-cytoskeleton-nucleus mechanotransduction pathway during endothelial cell rounding: axisymmetric model. Journal of Biomechanical Engineering 127(4):594-600.

[56] Hochmuth RM, Mohandas N, Blackshear Jr PL (1973) Measurement of the elastic modulus for red cell membrane using a fluid mechanical technique. Biophysical Journal 13(8):747-62.

[57] Eshelby J (1957) The determination of the elastic field of an ellipsoidal inclusion, and related problems. Proceedings of the Royal Society London, Series A 241: 376–396.

[58] Mori T, Tanaka K (1973) Average stress in matrix and average elastic energy of materials with misfitting inclusions. Acta Metallurgica 21(5):571-574.

[59] Satcher RL, Dewey CF (1996) Theoretical estimates of mechanical properties of the endothelial cell cytoskeleton. Biophysical Journal 71:109–118.

[60] Ingber, D. E., Heidemann, S. R., Lamoureux, P., and Buxbaum, R. E., 2000, “Opposing Views on Tensegrity as a Structural Framework for Understanding Cell Mechanics,” J. Appl. Physiol., 89, pp. 1663–1678.

[61] Kohn JC, Abdalrahman T, Sack KL, Reinhart-King CA, Franz T. (2018) Endothelial cells on an aged subendothelial matrix display heterogeneous strain profiles in silico, Biomechanics and Modeling in Mechanobiology 17: 1405 – 1414.

[62] Kohn, Julie C., et al. "Cell focal adhesion clustering leads to decreased and homogenized basal strains." International journal for numerical methods in biomedical engineering (2019): e3260.

[63] Milner JS, Grol MW, Beaucage KL, Dixon SJ, Holdsworth DW (2012) Finite-element modeling of viscoelastic cells during high-frequency cyclic strain. Journal of Functional Biomaterials3(1):209-24.

[64] Vernerey FJ, Farsad M (2014) A mathematical model of the coupled mechanisms of cell adhesion, contraction and spreading. Journal of Mathematical Biology 68(4):989-1022.

[65] Petroll WM, Cavanagh HD, Barry P, Andrews P, Jester JV (1993) Quantitative analysis of stress fiber orientation during corneal wound contraction. Journal of Cell Science 104(2):353-63.

[66] Sbrana F, Sassoli C, Meacci E, Nosi D, Squecco R, Paternostro F, Tiribilli B, Zecchi-Orlandini S, Francini F, Formigli L (2008) Role for stress fiber contraction in surface tension development and stretch activated channel regulation in C2C12 myoblasts. Am J Physiol Cell Physiol 295(1):C160–C172

[67] Caille N, Thoumine O, Tardy Y, Meister JJ (2002) Contribution of the nucleus to the mechanical properties of endothelial cells. Journal of Biomechanics 35(2):177-87.

[68] Ferko MC, Bhatnagar A, Garcia MB, Butler PJ (2007) Finite-element stress analysis of a multicomponent model of sheared and focally-adhered endothelial cells. Annals of Biomedical Engineering 35(2):208-23.